Post-synthesis modification of functionalised polyhedral oligomeric silsesquioxanes with encapsulated fluoride – enhancing reactivity of T 8 -F POSS for materials synthesis

Mathilde Laird, Philippe Gaveau, Philippe Trens, Carole Carcel, Masafumi Unno, John R Bartlett, Michel Wong Chi Man

Post-synthesis modification of functionalised polyhedral oligomeric silsesquioxanes with encapsulated fluoride – enhancing reactivity of T8-F POSS for materials synthesis

Mathilde Laird,[a] Philippe Gaveau,[a] Philippe Trens,[a] Carole Carcel,[a] Masafumi Unno,[b] John R. Bartlett*[c] and Michel Wong Chi Man*[a]

[a] *ICGM, Univ. Montpellier, CNRS, ENSCM, Montpellier, France. E-mail: michel.wong-chi-man@enscm.fr*
[b] *Department of Chemistry and Chemical Biology, Graduate School of Science and Technology, Gunma University, Kiryu 376-8515, Gunma, Japan*
[c] *Western Sydney University, Locked Bag 1797, Penrith, NSW 2751, Australia. E-mail: j.bartlett@westernsydney.edu.au*

Abstract
Previous studies have demonstrated that functionalised T_8 polyhedral oligomeric silsesquioxanes with fluoride anions encapsulated within the T_8 cage (T_8-F) have very low reactivity, with no reports of successful modification of the organic moieties. Herein, we report the successful modification of a styryl functionalised T_8-F compound with mercaptopropyltriethoxysilane using a thiol–ene click reaction. This strategy enables the vinyl moiety to be modified while maintaining the influence of the electron-withdrawing phenylene group, which stabilises the fluoride within the cage. The triethoxysilylated T_8-F cages were subsequently converted into nanohybrids by sol–gel processing. Multinuclear NMR experiments (^{29}Si, ^{19}F, ^{13}C) demonstrated that the POSS cage remained intact during both post functionalisation of T_8-F and subsequent sol-gel processing. Furthermore, ^{29}Si cross polarisation solid state NMR experiments using ^{19}F as a cross polarisation agent demonstrated that the fluoride anions remain localised within the cages in the nanohybrids. The functionalisation of the styryl bearing T_8-F POSS cage is the first example of both the successful modification of the poorly reactive T_8-F family and the formation of a nanohybrid material incorporating fluoride ions immobilised within covalently bound T_8 cages.

1. Introduction

Since their discovery in the 1940s and 1950s,[1,2] polyhedral oligomeric silsesquioxanes (POSS) have commanded significant interest within the chemistry, biomedical and materials communities. The T_n POSS family, also referred as T_n cage silsesquioxanes, are composed of a polyhedral silsesquioxane cage, $(SiO_{1.5})_n$, with functional organic branches covalently bonded to the vertices of the cage. The value of n can vary from n = 8, 10, 12, etc., with T_8 compounds (featuring a central void of 0.3 to 0.5 nm[3–5]) being the most commonly described. The organic moieties direct the functionalisation and reactivity of Tn compounds, and enable the cages to be modified by a palette of reaction including metathesis,[6–8] Heck coupling,[9,10] hydrosilylation,[11] thiol–ene click[12–14] or polymerisation.[15–18] A diverse range of applications for T_n cage systems have now been investigated, including bio/nanomedicine,[19–25] catalysis,[26–29] optoelectronics,[30] polymer chemistry,[31–33] and optical and sensing applications.[33–36] Postfunctionalised T_n compounds have also been incorporated into self-organised systems,[37–41] organic polymer-based nanohybrids,[31,33,42–45] POSS micelles and templated POSS systems leading to mesoporous materials with embedded T_8 cages.[46–48] In 2003, Bassindale's group reported a new T_8 cage silsesquioxane, in which a fluoride anion was entrapped within the central T_8 void, leading to the emergence of the T_8-F POSS family.[49] It was subsequently demonstrated that such compounds can be obtained when the T8 cage is functionalised with electron-withdrawing organic groups, but not with electron-donating species.[50] For example, in the case of electron-donating sp^3-hybridised organic groups, T_8 cages without encapsulated fluoride were obtained while with electronwithdrawing sp^3 or

sp^2 hybridised groups, T_8-F compound were formed. In addition, attempts to modify the organic substituents linked to the T_8-F cage via reactions typically used in organic synthesis were found to be unsuccessful.[51] To the best of our knowledge only one report of the modification of organic moieties linked to T_8-F cages, using electrochemical techniques, has appeared.[52] However, the integrity of the T_8-F cages was not demonstrated,[52] and no additional examples of successful modification of intact T_8-F cages could be found. A consequence of the difficulties encountered with post-functionalisation of the T_8-F family has been limited progress in exploring potential applications for such compounds over the past two decades. In a previous study, we reported the synthesis of new styryl-based cage silsesquioxanes (T_n with n = 8, 10, 12[53] or 18[54]), where the styryl group is bonded to all n vertices of the cages via the phenylene moiety. Subsequently, we described the preparation of the corresponding styryl-functionalised T_8-F compound,[55] whose formation was facilitated by the presence of the electron-withdrawing group linked to the vertices of the T_8 host. Herein, we investigate different potential approaches to functionalise the T_8-F cage and describe the successful modification of the styryl-bearing T_8-F molecule via grafting of a triethoxysilyl moiety using a thiol–ene click reaction,[56,57] without loss of fluoride from the T_8-F cage. The styryl/thiol–ene platform enables a much wider variety of reactive functional groups to be grafted onto the T_8-F cage, including electron-donating groups that cannot usually be covalently bound to T_8-F. We then demonstrate an example of potential approaches[57] for converting the reactive modified T_8-F precursor into a material, using sol–gel processing to produce an organic-inorganic hybrid in which the T_8-F cages remain intact. To the best of our knowledge, this constitutes the first report of a material incorporating intact T_8-F cage silsesquioxanes.

2. Experimental

2.1 Chemicals and purification methods

Tetrabutylammonium fluoride (TBAF, 1 M solution in THF (containing 5% H_2O)), (4-vinylphenyl)trimethoxysilane and dichloromethane (DCM, Analytical Grade) were obtained from Sigma Aldrich, TCI and VWR, respectively, and were used without further purification. Azobisisobutyronitrile (AIBN) was purchased from Sigma-Aldrich and was recrystallised. 3-Thiopropyltriethoxysilane was purchased from Fluorochem and was distilled prior to use. All syntheses were undertaken using HPLC-quality water.

2.2 Synthesis of triethoxysilylated functionalised T_8-F from styryl-functionalised T_8-F

The synthesis of styryl-functionalised T_8-F has been previously described.[55] In a flame dried Schlenk flask equipped with a Teflon rotaflos tap, styryl-functionalised T_8-F (250 mg, 167 mmol, 1 eq.) and AIBN (10.5 mg, 64.0 mmol, 0.5 mol%) were dissolved in dry chloroform (2.5 mL) under an inert atmosphere. The mixture was heated to 40 °C. 3-Thiopropyltriethoxysilane (320 mL, 1.33 mmol, 8 eq.) was then added dropwise and the temperature was increased to 60 °C. The mixture was stirred at 60 °C overnight and the solvent was then evaporated. The excess of 3-thiopropyltriethoxysilane was removed by washing the oil product with dry pentane. The excess of solvent was finally evaporated to yield a yellowish oil in nearly quantitative yield. 1,3,5,7,9,11,13,15-Octakis(4-(2-((3-(triethoxysilyl)propyl)thio)ethyl)-phenyl)-2,4,6,8,10,12,14,16,17,18,19,20-dodecaoxa-1,3,5,7,9,11,13,15-octasilapentacyclo[9.5.1.13,9.15,15.17,13]icosane fluoride, tetrabutylammonium salt ($C_{152}H_{268}O_{36}Si_{16}S_8NF$, yellowish oil): ^{1}HNMR (400 MHz, $CDCl_3$, δ, ppm): 7.73–7.71 (δ, C**H**$_{ar}$, 16H, J = 7.8 Hz), 7.10–7.08 (δ, C**H**$_{ar}$, 16H, J = 7.8 Hz), 3.83–3.78 (q, Si-O-C**H**$_2$-CH_3, 48H, J = 7.0 Hz), 2.82–2.80 (t, Ph-C**H**$_2$-CH_2-S, 16H, J = 4.5 Hz), 2.73–2.69 (t, Ph-CH_2-C**H**$_2$-S, 16H, J = 4.5 Hz), 2.59–2.55 (t, S-CH_2-C**H**$_2$-CH_2-Si, 16H, J = 7.4 Hz), 2.27 (m, NBu_4, 8H), 1.75–1.67 (quint, S-CH_2-C**H**$_2$-CH_2-Si, 16H, J = 7.4 Hz), 1.23–1.19 (q, Si-O-CH_2-C**H**$_3$, 72H, J = 7.0 Hz), 0.83 (m, NBu_4, 8H), 0.76–0.72 (t, S-CH_2-CH_2-C**H**$_2$- Si, 16H, J = 7.4 Hz), 0.69 (m, NBu_4, 12H). ^{13}C NMR (100 MHz, $CDCl_3$, δ, ppm): 140.94 (C_{ar}), 135.55 (C_{ar}), 134.75 (CH_{ar}), 127.29 (CH_{ar}), 58.40 (ethoxy, NBu_4), 36.55 (Ph-CH_2), 35.20 (CH_2-S), 33.41 (CH_2-S), 23.54 (NBu_4), 23.24 (CH_2), 19.46 (NBu_4), 18.34 (ethoxy), 13.68 (NBu_4), 9.95 (Si-CH_2). ^{19}F NMR (380 MHz, $CDCl_3$, δ, ppm): -

25.16. ^{29}Si NMR (80 MHz, $CDCl_3$, δ, ppm): -45.79 ($Si(OEt)_3$), -81.39 (cage, δ, J = 2.4Hz). IR(ν, cm^{-1}): 2973–2884 (CH_2 and CH_3), 1605 (C–C ring), 1072 (Si–O–Si).

MALDI-MS: *m/z*: calculated for (M + Na + H): 3188.1; found: 3188.0 (N.B.: during acquisition of the MALDI-MS spectrum, a cation exchange process occurs, resulting in substitution of the TBA^+ ion by a sodium ion. The observed *m/z* is thus characteristic of (M + Na + H) rather than the expected (M + TBA)).

2.3 Synthesis of T8-F gel

In a flame dried Schlenk flask, the solution of triethoxysilylated T_8-F cage in chloroform (568.0 mg, 0.166 mmol, 1 eq.) was evaporated and then dissolved in dry THF (2.0 mL). Water (24 mL, 1.3 mmol, 8 eq.) and TBAF (27 mL, 27 mmol, 0.16 eq.) were then successively added under stirring. After 3 min, the agitation ceased due to the rapid gelation of the mixture. After three days of ageing, the solid was crushed and washed three times with water and then acetone. The product was dried overnight under vacuum and recovered as a yellowish powder (350 mg). T_8-F Gel (yellowish powder): ^{13}C NMR (75 MHz, CP-MAS, δ, ppm): 140.5 (C_{ar}), 134.8 (CH_{ar}), 127.3 (CH_{ar}), 58.6 (residual ethoxy), 35.4, 24.0, 13.0. $_{19}$F NMR (565 MHz, δ, ppm): -21.9. ^{29}Si NMR (60 MHz, δ, ppm): -60.0 (alkylene T^2), -66.4 (alkylene T^3), -79.3 (cage). IR (ν, cm^{-1}): 1606 (C–C ring), 1066 (Si–O–Si).

2.4 Characterisation methods

FTIR spectra were recorded from 650 to 4000 cm^{-1} using a PerkinElmer Spectrum 100 equipped with a Gladia-ATR accessory. MALDI-MS spectra were acquired using a Bruker RapifleX spectrometer with dithranol/sodium trifluoroacetate as desorption matrix. Liquid ^{1}H, ^{13}C, ^{19}F and ^{29}Si NMR spectra were recorded on a Bruker Avance 400 MHz spectrometer in $CDCl_3$ at room temperature and at concentrations of around 10 mg mL^{-1}. ^{29}Si[^{1}H] and ^{13}C[^{1}H] solid-state NMR spectra were obtained on a VARIAN VNMRS 300 MHz spectrometer. ^{29}Si[^{1}H] CP-MAS (cross polarisation magic angle spinning) spectra were recorded with a 5 ms contact time, a 5 s recycle delay and a 6 kHz spinning rate. For ^{13}C[^{1}H] CP-MAS spectra, a contact time of 0.5 ms, a recycle delay of 3 s and spinning rate of 12 kHz were used. ^{19}F and ^{29}Si[^{19}F] solid-state NMR spectra were measured on a VARIAN VNMRS 600 MHz spectrometer. ^{19}F spectra were acquired using SP-MAS (single pulse magic angle spinning) techniques with a 3 μs $\pi/2$ pulse, a 60 s recycle delay and a 25 kHz spinning rate. For ^{29}Si[^{19}F] CP-MAS spectra, a contact time of 15 ms, a recycle delay of 10 s and spinning rate of 8 kHz were used. On both spectrometers, spectra were acquired using a 3.2 mm VARIAN T3 MAS probe with ZrO_2 rotors and were calibrated using secondary references: Q_8M_8H (octa(dimethylsiloxy)- octasilsesquioxane) for ^{29}Si (left line at -2.25 ppm); adamantane for ^{13}C (left line at 38.5 ppm); and PTFE (polytetrafluoroethylene) for ^{19}F (line at -122.3 ppm).

Thermogravimetric analyses (TGA) were carried out between 25 and 900 °C, using a heating rate of 10 °C min^{-1}. The gel samples were analysed using a TA Instruments Q50 apparatus with an air flow of 60 mL min^{-1} (T_8 and T_8-F gels), while the styryl-functionalised T_8-F POSS was analysed using a Netzsch STA 409 Luxx® instrument in static air. A Micromeritics ASAP 2020 instrument was used for the determination of nitrogen physisorption isotherms at -196 °C. The samples were activated at 100 °C for 3 days under secondary vacuum prior to analysis. Transmission electron microscopy (TEM) images were recorded on a JEOL 1400 + microscope operating at 120 kV with a LaB_6 source. Samples were prepared by deposition on Formvar/ Carbon 300 MeshTEM grids (FCF300-Cu-50).

3. Results and discussion

3.1 Functionalisation of octastyryl T8-F

As indicated above, there has been only one prior report addressing the post-functionalisation of the T_8-F system via electrochemical techniques, although the integrity of the T_8-F cage was not demonstrated in that earlier work.[52] Indeed, in allreports to date, reactions that have been successfully used to modify organic ligands on organo-functionalised T_n POSS compounds have led to the degradation of the POSS cage in the case of T_8-F compounds. For example, Taylor et al. Investigated the use of bromination, hydrosilylation, cycloaddition and cross metathesis reactions of the vinyl group on a vinyl-functionalised T_8-F compound.[51] The former two reactions resulted in the degradation of the cage, while the fluoride was found to deactivate the alkene dienophile of the addition reaction. In the case of the metathesis reaction, it was assumed that the TBA^+ cation led to deactivation of the Grubbs catalyst, thus preventing the reaction from proceeding.[51] In our work, preliminary scoping experiments using hydrosilylation and Heck coupling reactions led to a mixture of impure compounds, and hence these approaches were not pursued further (ESI,† Fig. S1–S3). Similarly, although the metathesis reaction yielded a modified product, characterisation studies indicated that the structure of the T_8-F cage had been modified (ESI,† Fig. S4 and S5), and hence this strategy was also abandoned. In contrast, preliminary experiments involving the use of a thiol–ene click reaction suggested that this strategy could be used to modify the vinyl group without degrading the T_8-F cage. Indeed, the fluoride anion remains entrapped within the cage due to the presence of the electron-withdrawing phenylenemoiety. Accordingly, we investigated the functionalisation of the styryl-functionalised T_8-F cage with 3-thiopropyltriethoxysilane using a thiol–ene click reaction, as shown in Fig. 1, to produce a triethoxysilylated derivative.

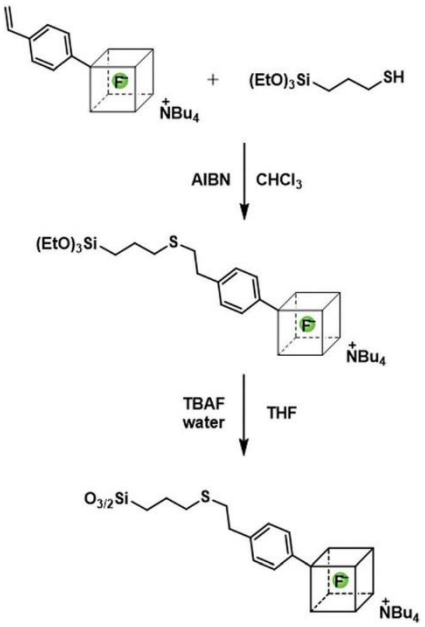

Fig. 1 Synthesis of triethoxysilylated T_8-F cage via thiol–ene click reaction and production of hybrid silica gel. For clarity, the functional group is shown on only one vertex of the cages.

Our initial approach followed a procedure described by Bivona et al.,[28] using toluene as a solvent. However, due to the low solubility of styryl-functionalised T_8-F in toluene, the reaction was carried out in dry chloroform, with AIBN as the radical initiator. The MALDI mass spectrum of the product obtained, Fig. S6 (ESI†), exhibits a peak at 3188.0 *m/z*, which is attributed to an adduct formed between the target molecule (3164.1 *m/z*), Na and H (M + Na + H, expected *m/z* = 3188.1). The ^{1}H solution NMR spectrum of the product obtained (Fig. 2), illustrates the loss of the signal arising from the vinylic protons at around 6.7 ppm (Fig. S7, ESI,† [55]), together with the appearance of new signals at 2.81 and 2.72 ppm arising from the –S–CH_2–CH_2– moiety, indicating completion of the thiol–ene click reaction and functionalisation of all eight styryl groups. The signals arising from the aromatic protons are also shifted from 7.73 and 7.31 ppm for the styryl-functionalised T_8-F cage to 7.72 and 7.09 ppm,

respectively, for the triethoxysilylated product. Signals arising from the propyl moiety are observed at 2.57, 1.71 and 0.74 ppm together with those of the ethoxy groups at 3.80 and 1.22 ppm. It should be noted that a singlet observed at around 1.71 ppm, which overlaps the signals associated with the propyl group, arises from AIBN. In addition, the signals associated with the TBA^+ counter ion are still seen at 2.26, 0.80 and 0.68 ppm. The integration of the various signals is consistent with the proposed product (Fig. 2).

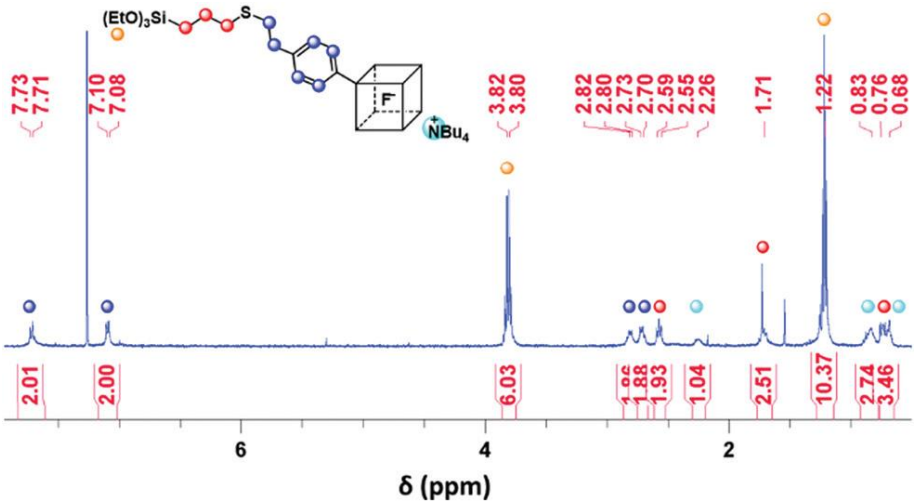

Fig. 2 Solution ^{1}H NMR spectrum of the triethoxysilylated functionalised T_8-F cage. For clarity, the functional group is shown on only one vertex of the cages.

^{19}F solution NMR spectroscopy confirms the retention of the fluoride in the cage (Fig. 3 and Fig. S8, ESI†), with the signal observed at -25.16 ppm being characteristic of the T_8-F cage.[49,51,55,58] In particular, styryl-functionalised T_8-F exhibits a signal at-25.17 ppm[55] prior to thiol–ene grafting. Additional signals are also evident on the base of the main peak, with the strongest of these being observed at -25.43 ppm. The complete conversion of the vinyl groups initially present on the styryl-functionalised T_8-F confirms that the latter signal does not arise from a partially functionalised cage (i.e. all eight styryl groups have been functionalised). Although these weak signals cannot be unambiguously attributed on the basis of the available data, their chemical shifts confirm that they still correspond to an encapsulated fluoride anion, and they are tentatively assigned to oligomeric species arising from styryl oligomerisation catalysed by AIBN (see Section 1.5 in the ESI†).

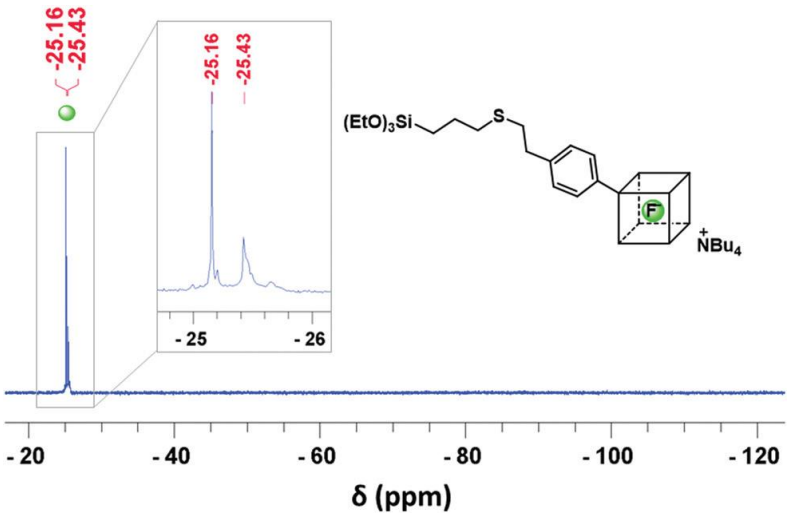

Fig. 3 Solution ^{19}F NMR spectrum of the triethoxysilylated functionalised T_8-F cage. For clarity, the functional group is shown on only one vertex of the cages.

The ^{29}Si solution NMR spectrum (Fig. 4 and Fig. S9, ESI†) is also consistent with the formation of the expected product. A signal arising from the triethoxysilylated moiety is observed at -45.79 ppm, while that associated with the silsesquioxane cage is seen as a doublet at -81.39 ppm (JSi–F = 2.4 Hz). The latter chemical shift and coupling constant are similar to those observed for the styryl-functionalised T_8-F (-81.49 ppm; JSi–F = 2.5 Hz, Fig. S9, ESI,† [55]). Weak signals associated with small quantities of by-products and impurities are also observed at the base of the signals arising from the T_8-F cage, which probably arise fromoligomeric species associated with the ^{19}F NMR signal observed at -25.43 ppm.

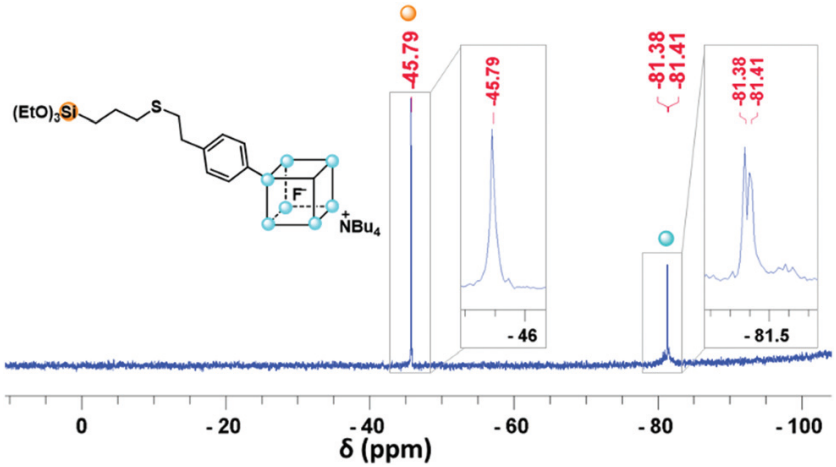

Fig. 4 Solution ^{29}Si NMR spectrum of the triethoxysilylated functionalised T_8-F cage. For clarity, the functional group is shown on only one vertex of the cages.

The FTIR spectrum of the product (Fig. S10, ESI†) is also consistent with the proposed structure. In particular, a sharp Si–O–Si stretching band at 1072 cm^{-1}, characteristic of a well-defined cage silsesquioxane is observed, which is similar to that previously reported for the styryl-functionalised T_8-F compound.[55] The loss of the CQC stretching mode at 1628 cm^{-1} associated with the vinyl group initially present on the styryl moiety is consistent with the hydrothiolation of the double bond. In addition, a weak peak is observed at 692 cm^{-1} (see inset to Fig. S10, ESI†) which is tentatively assigned to the C–S stretching mode.[59,60] The weak peak observed at around 3680 cm^{-1} is attributed to small quantities of isolated silanol species, which were presumably formed by hydrolysis of the ethoxy groups during acquisition of the spectra and associated exposure to atmospheric moisture. The flat spectral response observed from 3100 to 3600 cm^{-1} indicates that there are no H-bonded water, alcohol, or H-bonded silanol species in the precursor. In addition, a weak signal arising from the minor hydrolysis product can be observed in the ^{29}Si NMR spectrum of the precursor, upfield to the main T^0 peak at -45.69 ppm, when the sample is exposed to atmospheric water vapour. The intensity of the weak signal (not seen in Fig. 4) increases with increasing exposure to atmospheric moisture, confirming that it is not an intrinsic feature of the precursor compound and is an artefact arising from hydrolysis. Finally, a possible attribution of the minor signals observed in the ^{29}Si and ^{19}F NMR spectra (at -81.58 and -25.43 ppm, respectively) to the small quantity of hydrolysed species observed by FTIR may be discounted, in view of the fact that these hydroxyls are located more than 10 atoms distant from the silsesquioxane cage.

3.2 Formation of gels incorporating intact T8-F silsesquioxane cages

As indicated above, there now exists a rapidly growing body of work on the incorporation of functionalised T_n cages into a variety of materials, with many such systems and corresponding

applications summarised in a recent review.[33] However, materials incorporating intact T_8-F cages have not been unambiguously demonstrated previously. Hence a key goal of this work was to highlight an example of the successful conversion of the reactive precursor produced via the styryl/thiol–ene reaction platform into a nanohybrid material with retention of the T_8-F moieties. Accordingly, we next investigated the fluoride-catalysed conversion of the precursor into a gel via sol–gel processing, as illustrated in Fig. 1.

The TEM micrograph of the material obtained, Fig. S11 (ESI†), is consistent with a dense, relatively uniform structure, with no porosity being evident. This was confirmed by N_2 physisorption, with the low quantities of gas adsorbed precluding any meaningful analysis of porosity or surface area.

Retention of the fluoride species within the T_8 cages embedded in the hybrid network was confirmed by ^{19}F SP-MAS NMR spectroscopy, which revealed a single broad signal centred at -21.9 ppm (Fig. 5, top). This is shifted downfield compared to the chemical shift of the styryl-functionalised T_8-F (-25.17 ppm[55]) and the triethoxysilylated precursor (-25.16 ppm, Fig. 3) in the corresponding solution NMR spectra. The width of the signal compared to the solid state NMR signal of the styryl T8-F,55 together with the asymmetry on the downfield side, also suggests that the T_8-F cages experience a range of different environments within the gel matrix, consistent with a disordered gel structure. A broad signal is also evident at -132.0 ppm (Fig. S12, ESI†), which is attributed to residual TBAF not removed during washing of the gel, following earlier reports of a similar feature at -129 ppm in the ^{19}F NMR spectrum of a POSS system incorporating TBAF.[61]

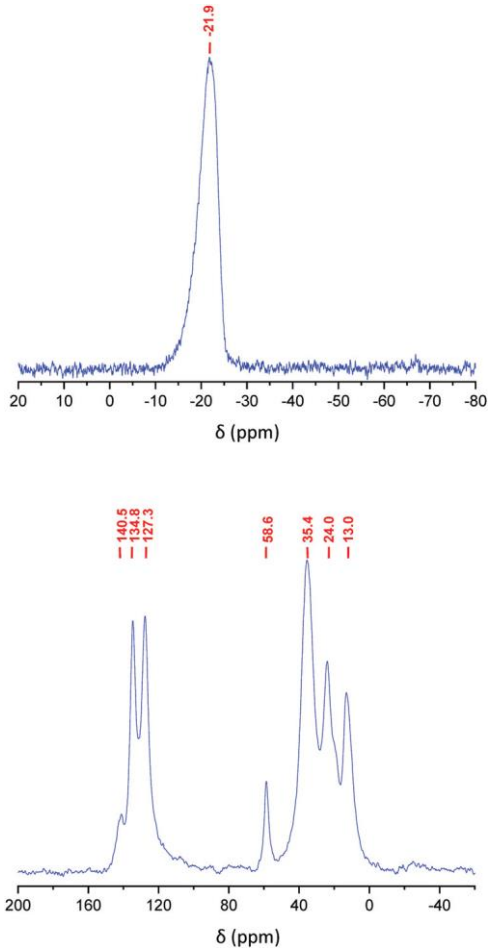

Fig. 5 ^{19}F SP-MAS (top) and ^{13}C CP-MAS (bottom) solid state NMR spectra of the T_8-F gel.

The ^{13}C CP-MAS NMR spectrum of the gel (Fig. 5, bottom) exhibits the expected signals arising from the phenylene moiety linked to the T_8-F cage at 140.5, 134.8 and 127.3 ppm.[55] Aliphatic CH_2 groups from the ethyl and propyl branches (the latter arising from the thiopropyl moiety), together with the TBA^+ cation, are also observed as a cluster of signals between 35.4 and 13.0 ppm. In addition, the spectrum indicates that hydrolysis is not complete, as demonstrated by the presence of signals arising from residual ethoxy groups at 58.6 ppm and in the aliphatic signal cluster between 35.4 and 13.0 ppm.

Silicon species associated with both the gel matrix and the intact T_8-F cage are clearly evident in the ^{29}Si MAS spectra of the gel (Fig. 6). In particular, the spectrum obtained by cross polarisation using the ^1H nucleus (Fig. 6, middle) exhibits signals associated with T^2 (R–Si(OX)O, X = H, Et) and T^3 (R–$SiO_{1.5}$) species at -60.0 and -66.4 ppm, which arise from hydrolysis and condensation of the thiopropyltriethoxysilylated moiety. An additional signal associated with this network is also observed as a weak shoulder downfield to the T^2 signal, which is attributed to the corresponding T^1 species. The observation of T^2 and T^1 species is consistent with the ^{13}C NMR spectrum, which indicated that hydrolysis was not complete. The additional narrow signal observed at -79.3 ppm is unambiguously attributed to the T^3 Si species, functionalised with aromatic moieties, that comprise the fully intact T_8-F silsesquioxane cages. It is interesting that the chemical shift observed for these latter species is shifted downfield compared to the values obtained for styryl-functionalised T_8-F (-80.72 and -81.2355), as previously observed for the corresponding T_8 and T_{10} gel systems.[57] This deshielding is also similar to that observed in the associated ^{19}F solid-state NMR spectrum. The ^1H cross polarised ^{29}Si NMR spectrum of the corresponding T_8 gel[57] is also shown for comparison in Fig. 6 (top). It should be noted that the T_8 gel was prepared under acid-catalysed conditions, whereas the T_8-F product was prepared using nucleophilic catalysis. As expected, the relative abundance of aliphatic T^3 species in the case of the T_8-F gel is higher than that in the T_8 gel (where T^2 and T^1 species predominate), due to the higher extent of condensation expected for nucleophilic catalysis compared to acid-catalysed conditions.[62] The T_8 cage resonance for the T_8 gel (-76.3 ppm) is also downfield with respect to that of the T_8-F cage (-79.3 ppm), as is typically observed for these systems in liquid NMR spectroscopy.[55]

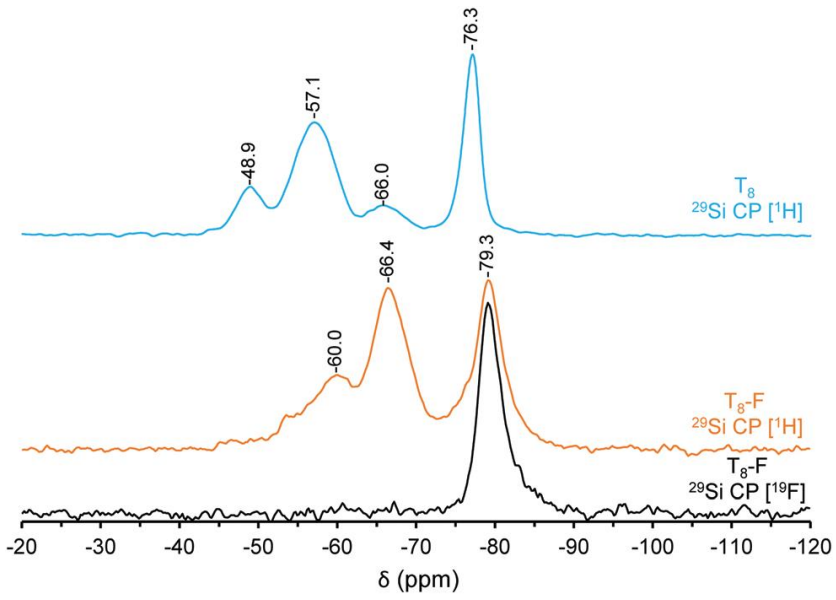

Fig. 6 ^{29}Si CP [^1H] of the T_8 gel (top[57]); compared with ^{29}Si CP [^1H] (middle) and ^{29}Si CP [^{19}F] (bottom) MAS solid state NMR spectra of the T_8-F gel.

In order to unambiguously confirm the retention of the fluoride ion within the T_8 cage of the T_8-F gel, an additional solid state ^{29}Si cross polarisation NMR experiment was performed using the fluoride signal observed at -21.9 ppm in the ^{19}F NMR spectrum for polarisation transfer (Fig. 6, bottom). In this latter ^{29}Si CP-MAS NMR experiment, a single signal at -79.3 ppm can be seen. This signal

corresponds to the T^3 silicon species of the T_8-F cage and appears at the same chemical shift as in the corresponding ^{29}Si CP-MAS NMR spectrum with ^{1}H polarisation transfer (Fig. 6, middle). In addition, as expected, the T^2 and T^3 signals associated with the hydrolysed triethoxysilyl group are no longer observed when using ^{19}F as the polarisation transfer nucleus, since the corresponding silicon atoms do not interact with the fluoride anion. These observations further confirm the retention of the fluoride in the T_8-F cages and show that the cage was not degraded during the synthesis of the gel.

In our earlier study,[55] we demonstrated the enhanced stability of the styryl-functionalised T_8-F POSS under conditions that had been previously shown to release the fluoride anion from the POSS cage in other T_8-F compounds. This stability might also contribute to the retention of the fluoride ion within the intact POSS structure during the thiol–ene click reaction and subsequent sol–gel processing.

Thermal decomposition of POSS compounds has been the subject of several studies.[63–66] For example, octaphenylfunctionalised T_8 POSS was found to retain 95% of its initial mass up to 471 °C under an air atmosphere, with substantial decomposition subsequently observed from 500 to 700 ° C by Blanco et al.[63] A similar result was reported by Fan and Yang,[64] who indicated that the onset of thermal decomposition was 465 °C in the octaphenyl T_8 POSS system. T_8 silsesquioxane cages functionalised with aliphatic groups such as aminopropyl chains also exhibit relatively high decomposition temperatures, with the onset of decomposition of the POSS cage being observed at around 425 °C.[65] In this latter case, a mass loss at lower temperatures (<200 °C) was attributed to the desorption of water bound to the hydrophilic aminopropyl groups. A model to predict the onset of thermal decomposition in organo-functionalised T_8 POSS compounds has also been reported.[66] However, as far as we are aware, there have been no reports of the thermal-decomposition characteristics of T_8-F POSS compounds.

The thermogravimetric analyses of T_8-F POSS, together with the T_8-F and T_8 gels, are compared in Fig. 7. As above, we note that the two gel samples were prepared using different sol–gel catalysts, although key differences in their respective TGA traces can be largely attributed to the presence of the encapsulated fluoride and TBA^+ counter-ion in the case of the T_8-F gel.

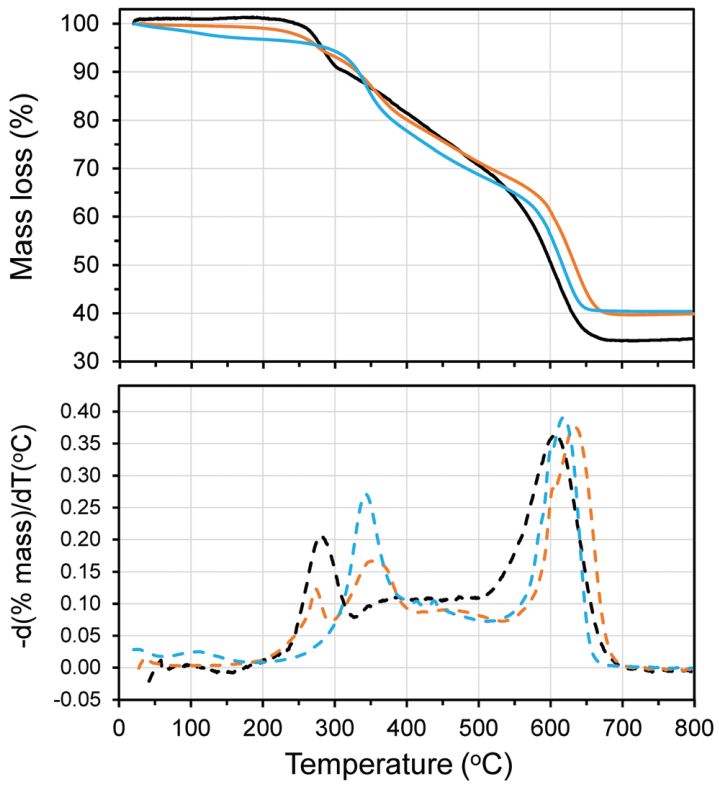

Fig. 7 TGA (top) and dTGA (bottom) of T_8 (blue) and T_8-F gels (orange); and T_8-F POSS precursor (black).

The ~3% mass loss below 200 °C in the case of the T_8 gel is attributed to the loss of ''structural'' water,[57] with a much smaller evolution being observed in the case of the T_8-F gel (<1%). No such mass loss is evident for T_8-F POSS below 200 °C, consistent with the lack of water associated with the compound. The feature at 275 °C in the case of the T_8-F gel (~6% mass loss) and T_8-F POSS (~11%) is not observed in the T_8 gel system and is attributed to the partial decomposition of the TBA^+ counter-ions, which account for 7 and 16% of the mass of the gel and T_8-F POSS, respectively. Similar TGA profiles have been previously reported for a range of TBA^+ compounds.[67–69] The feature at ~350 °C in the dTGA traces of the gels is much less prominent in the case of the T_8-F POSS, suggesting that it arises mainly from the loss of hydroxyl species in the gels, together with a minor contribution from decomposition of organics. This attribution is also consistent with the relative intensities of the corresponding T^1 and T^2 NMR signals for the T_8 and T_8-F gels (Fig. 6), with the larger hydroxyl content in the former sample giving rise to an increased mass loss in this region (Fig. 7).

The significant mass losses beginning at around 550 °C, and the associated maxima in the dTGA traces at ~600–630 °C for both gels and T_8-F POSS, contain contributions resulting mainly from the decomposition of organic species and the T_8 cages, both of which occur in multiple steps. The latter feature is similar to that typically observed for simple organo-functionalised T_8 POSS compounds.[63,64] The weak shoulder observed at around 600 °C in the dTGA plot of the T_8-F gel (which is not observed in the case of the T_8 gel) is tentatively attributed to loss of fluoride species following decomposition of the T_8 cages. Finally, the residual masses of the two gel samples at 800 °C (~40.4%) are comparable, while that of the T_8-F precursor (34.7%) is close to the value of 32.0% expected following decomposition and associated formation of SiO_2.

FTIR spectra of the triethoxysilyl T_8-F precursor and gel,together with the corresponding T_8 gel,[57] are compared in Fig. 8. The spectra were normalised against the intensity of the phenyl ring stretching band at 1604 cm^{-1}, since the phenyl ring is retained within the structure and not transformed during sol–gel processing. The broadening of the Si–O–Si stretching band at 1064 cm^{-1} in the gel is consistent with the formation of a disordered Si–O–Si network from the hydrolysiscondensation of the triethoxysilyl moiety, with the gel network being less organised than the Si–O–Si species within the cages. The decrease in the intensity of the CH_3 stretching mode at 2972 cm^{-1} is also consistent with the hydrolysis of the ethoxy groups. It should be noted that a component of the 2972 cm^{-1} peak is also associated with the TBA^+ counter-ions retained within the structure, which contributes to the spectroscopic profile in the C–H stretching region. In addition, the peak at 3680 cm^{-1} attributed to isolated silanol species in the T_8-F precursor is not evident in the spectrum of the corresponding gel, indicating that the majority of silanol species in the gel were condensed or are H-bonded.

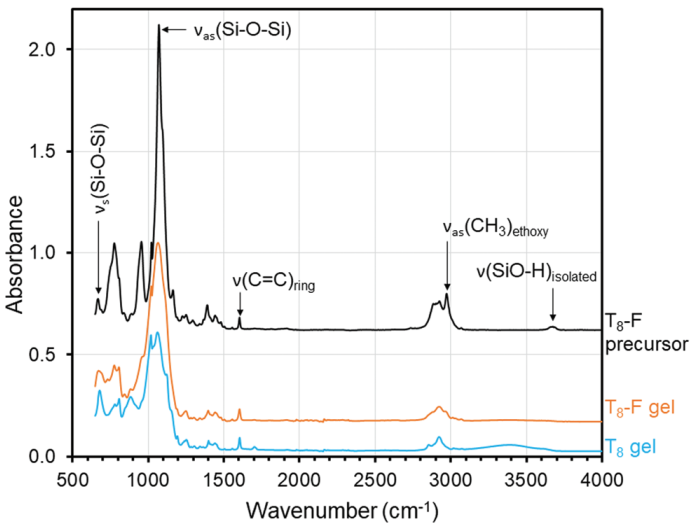

Fig. 8 FTIR spectra of the triethoxysilylated T_8-F precursor (top) and of the material obtained via sol–gel processing of the latter (middle), compared to that of the corresponding T_8 gel (bottom). All spectra were normalised to the intensity of the ν(C=C) mode.

Selected regions of the FTIR spectra of the T_8-F and T_8 gels are compared in greater detail in Fig. 9. The spectrum of the T_8 gel exhibits a band at 1704 cm^{-1} (Fig. 9, bottom), which was previously attributed by us to ''structural'' water strongly interacting with the silsesquioxane gel network.[57] Briefly, earlier studies of the vibrational spectrum of water in a variety of systems demonstrated that increasing H bond strength in water led to an increase in the wavenumber of the bending mode within the range <1600 to >1700 cm^{-1}.[70] Similar conclusions were reported in subsequent computational and experimental studies,[71] while a peak in the spectrum of zeolite NaA observed at 1678 cm^{-1} was attributed to ''connective'', ice like water within the zeolite cage.[72] It was noted that the properties of this ''connective'' water were significantly different to those of bulk water.[72] A similar peak is also observed in the spectrum of the T_8-F gel (Fig. 9, top) although it is significantly weaker, consistent with the presence of less water in the latter sample. Similar conclusions can be drawn from the corresponding broad ν(OH) profiles at 3400 cm^{-1}, where the profile intensity for the T_8-F gel is significantly weaker than that of the T_8 material. These results are consistent with the TGA data that indicate only small quantities of water are present in the T_8-F gel.

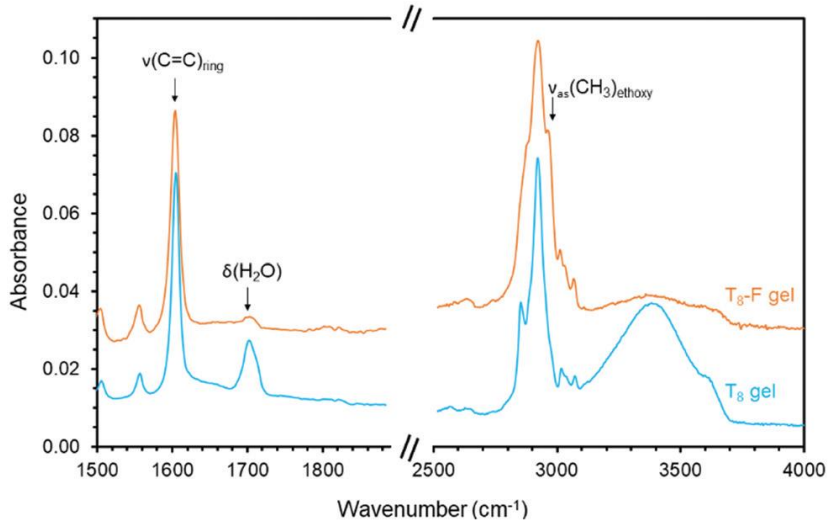

Fig. 9 Expanded view of the FTIR spectra shown in Fig. 8, highlighting the 1500 to 1900 (left) and 2500 to 4000 cm^{-1} regions (right).

The low water content of the T_8-F gel, despite the presence of the hydrophilic TBA^+ counter ion in the material, is intriguing. The structure of the styryl-functionalised T_8-F was reported in our earlier paper,[55] which revealed that the TBA^+ cation is surrounded by phenyl groups in the compound. Given the Si–F interaction observed in this system,[55] the negative charge is presumably partially delocalised across the eight phenyl rings, with each ring bearing a partial negative charge which is balanced by the proximate counter ion. A similar short-range structure would also be anticipated in the gel. This suggests that the low water uptake of the gel might be influenced by shielding of the hydrophilic TBA^+ cation and by the nearby hydrophobic phenyl groups.

Finally, to enhance the range of potential applications for such materials, the possibility of intentionally degrading the T_8-F cage to generate size-controlled porosity within the gel matrix was also considered. Cage silsesquioxanes are known to be cleaved under basic conditions, and hence preliminary experiments involving exposure of the gel to pyridine at ambient temperature were undertaken. However, ^{19}F SP NMR studies demonstrated that the attempt to cleave the cage was unsuccessful, with a signal still observed at -21.3 ppm and no new signals appearing. Additional experiments were undertaken with refluxing triethylamine, but no cleavage was observed under these more robust conditions either. These results suggest that the T_8-F cage is at least partially stabilised in the hybrid material, due to (a) the intrinsic stability of the styryl-functionalised T_8-F system; and/or (b) its incorporation within the dense gel matrix, which limits penetration of the base into the network.

4. Conclusions

In summary, despite the typically low reactivity of T_8-F compounds toward traditional organic synthesis reactions, the styryl-functionalised T8-F has been successfully modified via a thiol–ene click reaction with mercaptopropyltriethoxysilane. In particular, we demonstrate for the first time the successful post-functionalisation of a T_8-F compound without degradation of the POSS cage and with retention of the fluoride anion within the cage. A particular feature of this approach is that the styryl/thiol–ene platform enables a much wider variety of reactive functional groups to be grafted onto the T_8-F cage, including electron-donating groups that cannot usually be covalently bound to T_8-F. We note that the previous lack of such reactive T_8-F compounds has limited progress in exploring potential applications for this intriguing family of compounds over the past few decades.

To provide an example of potential approaches for incorporating the reactive T_8-F moieties within materials, we next explored the transformation of the triethoxysilylated T_8-F compound into a gel via sol–gel processing. Solid-state multinuclear NMR studies (^{29}Si, ^{19}F, ^{13}C) demonstrated that the POSS cage structure remains intact, with fluoride retained within the cage, after sol–gel processing and formation of the nanohybrid material. This latter feature was shown by cross polarisation ^{29}Si NMR sequences using ^{19}F as polarisation transfer agent, which demonstrated unambiguously that the fluoride remains encapsulated within the POSS cage after formation of the sol–gel silsesquioxane network. The resulting material thus contains nanometre-sized charged domains, uniformly incorporated within a nanohybrid network.

This is the first unambiguous example of reactive T_8-F precursors that can be used to covalently incorporate T_8-F POSS species within a functional material. Interestingly, TGA and IR analysis demonstrated that the material contained only small quantities of water, despite the presence of the hydrophilic TBA^+ cation within the matrix. This suggests a possible application for such materials as hydrophobic coatings, which remains to be explored. The availability of precursors for producing materials incorporating intact T_8-F moieties also opens the way to the preparation of new materials with properties such as electrical conductivity, optical response, etc., that can be modulated by the presence of encapsulated fluoride anions within their structure.

Conflicts of interest

There are no conflicts to declare.

Acknowledgements

The authors gratefully acknowledge Frank Godiard (Plateforme Microscopie Electronique et Analytique, Université de Montpellier) for TEM measurements, as well as Cédric Totée and Emmanuel Fernandez (Plateforme d'Analyses et de Caractérisation Balard – PAC Balard Montpellier) for NMR experiments. Funding from the French Ministère de l'Enseignement Supérieur et de la Rechercheto support the PhD scholarship of Mathilde Laird and the Japan Student Services Organization for a travel scholarship awarded to Mathilde Laird are gratefully acknowledged.

Notes and references

1 D. W. Scott, *J. Am. Chem. Soc.*, 1946, **68**, 356–358.
2 A. J. Barry, W. H. Daudt, J. J. Domicone and J. W. Gilkey, *J. Am. Chem. Soc.*, 1955, **77**, 4248–4252.
3 A. R. Bassindale, Z. Liu, I. A. MacKinnon, P. G. Taylor, Y. Yang, M. E. Light, P. N. Horton and M. B. Hursthouse, *Dalton Trans.*, 2003, 2945–2949.
4 N. Hurkes, C. Bruhn, F. Belaj and R. Pietschnig, *Organometallics*, 2014, **33**, 7299–7306.

5 M. A. Hossain, M. B. Hursthouse and K. M. A. Malik, *Acta Crystallogr., Sect. B: Struct. Sci.*, 1979, **B35**, 2258–2260.
6 D. B. Cordes, P. D. Lickiss and F. Rataboul, *Chem. Rev*., 2010, **110**, 2081–2173.
7 J. H. Jung, J. C. Furgal, T. Goodson, T. Mizumo, M. Schwartz, K. Chou, J. F. Vonet and R. M. Laine, *Chem. Mater.*, 2012, **24**, 1883–1895.
8 Y. Itami, B. Marciniec and M. Kabicki, *Chem. – Eur. J.*, 2004, **10**, 1239–1248.
9 M. Y. Lo, K. Ueno, H. Tanabe and A. Sellinger, *Chem. Rec.*, 2006, **6**, 157–168.
10 A. Sellinger, R. Tamaki, R. M. Laine, K. Ueno, H. Tanabe, E. Williams and G. E. Jabbour, *Chem. Commun.*, 2005, 3700–3702.
11 E.Markovic,M. Ginic-Markovic, S.Clarke, J.Matisons,M.Hussain and G. P. Simon, *Macromolecules*, 2007, **40**, 2694–2701.
12 K. Yue, C. Liu, K. Guo, X. Yu, M. Huang, Y. Li, C. Wesdemiotis, S. Z. D. Cheng and W. B. Zhang, *Macromolecules*, 2012, **45**, 8126–8134.
13 K. Hou, Y. Zeng, C. Zhou, J. Chen, X. Wen, S. Xu, J. Cheng and P. Pi, *Chem. Eng. J.*, 2018, **332**, 150–159.
14 F. Alves and I. Nischang, *Chem. – Eur. J.*, 2013, **19**, 17310–17313.
15 C. Zhang, F. Babonneau, C. Bonhomme, R. M. Laine, C. L. Soles, H. A. Hristov and A. F. Yee, *J. Am. Chem. Soc.*, 1998, **120**, 8380–8391.
16 D. Hoebbel, K. Endres, T. Reinert and I. Pitsch, *J. Non-Cryst. Solids*, 1994, **176**, 179–188.
17 J. J. Morrison, C. J. Love, B. W. Manson, I. J. Shannon and R. E. Morris, *J. Mater. Chem.*, 2002, **12**, 3208–3212.
18 Y. Hagiwara, A. Shimojima and K. Kuroda, *Chem. Mater.*, 2008, **20**, 1147–1153.
19 R. Y. Kannan, H. J. Salacinski, P. E. Butler and A.M. Seifalian, *Acc. Chem. Res.*, 2005, **38**, 879–884.
20 H. Ghanbari, B. G. Cousins and A. M. Seifalian, *Macromol. Rapid Commun.*, 2011, **32**, 1032–1046.
21 A. Solouk, B. G. Cousins, F. Mirahmadi, H. Mirzadeh, M. R. J. Nadoushan, M. A. Shokrgozar and A. M. Seifalian, *Mater. Sci. Eng., C*, 2015, **46**, 400–408.
22 L. Nayyer, M. Birchall, A. M. Seifalian and G. Jell, *Nanomedicine*, 2014, **10**, 235–246.
23 R. Y. Kannan, H. J. Salacinski, J. De Groot, I. Clatworthy,L. Bozec, M. Horton, P. E. Butler and A. M. Seifalian, *Biomacromolecules*, 2006, **7**, 215–223.
24 R. Y. Kannan, H. J. Salacinski, M. Odlyha, P. E. Butler and A. M. Seifalian, *Biomaterials*, 2006, **27**, 1971–1979.
25 M. Feghhi, J. Rezaie, A. Akbari, N. Jabbari, H. Jafari, F. Seidi and S. Szafert, *Mater. Des.*, 2021, **197**, 109227.
26 E. A. Quadrelli and J. M. Basset, *Coord. Chem. Rev.*, 2010, **254**, 707–728.
27 F. Giacalone and M. Gruttadauria, *ChemCatChem*, 2016, **8**, 664–684.
28 L. A. Bivona, F. Giacalone, E. Carbonell, M. Gruttadauria and C. Aprile, *ChemCatChem*, 2016, **8**, 1685–1691.
29 Y. Zhou, G. Yang, C. Lu, J. Nie, Z. Chen and J. Ren, *Catal. Commun.*, 2016, **75**, 23–27.
30 Z. Li, J. Kong, F. Wang and C. He, *J. Mater. Chem. C*, 2017, **5**, 5283–5298.
31 A. Kausar, *Polym.-Plast. Technol. Eng.*, 2017, **56**, 1401–1420.
32 D. Gnanasekaran, K. Madhavpan and R. S. R. Reddy, *J. Sci. Ind. Res.*, 2009, **68**, 437–464.
33 H. Zhou, Q. Ye and J. Xu, *Mater. Chem. Front.*, 2017, **1**, 212–230.
34 S. Chanmungkalakul, V. Ervithayasuporn, P. Boonkitti, A. Phuekphong, N. Prigyai, S. Kladsomboon and S. Kiatkamjornwong, *Chem. Sci.*, 2018, **9**, 7753–7765.
35 S. Chanmungkalakul, V. Ervithayasuporn, S. Hanprasit, M. Masik, N. Prigyai and S. Kiatkamjornwong, *Chem. Commun.*, 2017, **53**, 12108–12111.
36 C.Wannasiri, S. Chanmungkalakul, T. Bunchuay, L. Chuenchom, K. Uraisin, V. Ervithayasuporn and S. Kiatkamjornwong, *ACS Appl. Polym. Mater.*, 2020, **2**, 1244–1255.
37 N. Sato, Y. Kuroda, T. Abe, H. Wada, A. Shimojima and K. Kuroda, *Chem. Commun.*, 2015, **51**, 11034–11037.
38 A. Akbari, N. Arsalani, M. Amini and E. Jabbari, *J. Mol. Catal. A: Chem.*, 2016, **414**, 47–54.
39 S. Ko¨ytepe, M. H. Demirel, A. Gu¨ltek and T. Seçkin, *Polym. Int.*, 2014, **63**, 778–787.

40 A. Kowalewska, *Curr. Org. Chem.*, 2017, **21**, 1243–1264.
41 E. Heeley, Y. El Aziz, C. Ellingford, A. Jetybayeva, C. Wan, E. Crabb, P. G. Taylor and A. Bassindale, *CrystEngComm*, 2019, **21**, 710–723.
42 M. A. Chiacchio, L. Borrello, G. Di Pasquale, A. Pollicino, F. A. Bottino and A. Rescifina, *Tetrahedron*, 2005, **61**, 7986–7993.
43 T. S. Haddad, B. D. Viers and S. H. Phillips, *J. Inorg. Organomet. Polym.*, 2001, **11**, 155–164.
44 S. H. Phillips, T. S. Haddad and S. J. Tomczak, *Curr. Opin. Solid State Mater. Sci.*, 2004, **8**, 21–29.
45 A. Romo-Uribe, P. T. Mather, T. S.Haddad and J. D. Lichtenhan, *J. Polym. Sci., Part B: Polym. Phys.*, 1998, **36**, 1857–1872.
46 R. Goto, A. Shimojima, H. Kuge and K. Kuroda, *Chem. Commun.*, 2008, 6152–6154.
47 A. Shimojima, R. Goto, N. Atsumi and K. Kuroda, *Chem. – Eur. J.*, 2008, **14**, 8500–8506.
48 M. Seino, W. Wang, J. E. Lofgreen, D. P. Puzzo, T. Manabe and G. A. Ozin, *J. Am. Chem. Soc.*, 2011, **133**, 18082–18085.
49 A. R. Bassindale, M. Pourny, P. G. Taylor, M. B. Hursthouse and M. E. Light, *Angew. Chem., Int. Ed.*, 2003, **42**, 3487–3490.
50 Y. El Aziz, A. R. Bassindale, P. G. Taylor, P. N. Horton, R. A. Stephenson and M. B. Hursthouse, *Organometallics*, 2012, **31**, 6032–6040.
51 P. G. Taylor, A. R. Bassindale, Y. El Aziz, M. Pourny, R. Stevenson, M. B. Hursthouse and S. J. Coles, *Dalton Trans.*, 2012, **41**, 2048–2059.
52 A. Farhati, M. Syroeshkin, M. Dammak and V. Jouikov, *Electrochem. Commun.*, 2018, **95**, 5–8.
53 M. Laird, A. Van Der Lee, D. G. Dumitrescu, C. Carcel, A. Ouali, J. R. Bartlett, M. Unno and M. Wong Chi Man, *Organometallics*, 2020, **39**, 1896–1906.
54 M. Laird, N. Herrmann, N. Ramsahye, C. Totée, C. Carcel, M. Unno, J. R. Bartlett and M. Wong Chi Man, *Angew. Chem., Int. Ed.*, 2021, **60**, 3022–3027.
55 M. Laird, C. Totée, P. Gaveau, G. Silly, A. Van der Lee, C. Carcel, M. Unno, J. R. Bartlett and M. Wong Chi Man, *Dalton Trans.*, 2021, **50**, 81–89.
56 Y. Li, X. H. Dong, Y. Zou, Z. Wang, K. Yue, M. Huang, H. Liu, X. Feng, Z. Lin, W. Zhang, W. B. Zhang and S. Z. D. Cheng, *Polymer*, 2017, **125**, 303–329.
57 M. Laird, J. Yokoyama, C. Carcel, M. Unno, J. R. Bartlett and M. Wong Chi Man, *J. Sol–Gel Sci. Technol.*, 2020, **95**, 760–770.
58 Y. El Aziz, P. G. Taylor, A. R. Bassindale, S. J. Coles and M. B. Pitak, *Organometallics*, 2016, **35**, 4004–4013.
59 D. W. Scott and J. P. McCullough, *J. Am. Chem. Soc.*, 1958, **80**, 3554–3558.
60 M. Ohsaku, Y. Shiro and H. Murata, *Bull. Chem. Soc. Jpn.*, 1972, **45**, 113–121.
61 H. J. Ben, X. K. Ren, B. Song, X. Li, Y. Feng, W. Jiang, E. Q. Chen, Z. Wang and S. Jiang, *J. Mater. Chem. C*, 2017, **5**, 2566–2576.
62 J. J. E. Moreau, L. Vellutini, M. Wong Chi Man, C. Bied, P. Dieudonné, J. L. Bantignies and J. L. Sauvajol, *Chem. – Eur. J.*, 2005, **11**, 1527–1537.
63 I. Blanco, L. Abate and F. A. Bottino, *Thermochim. Acta*, 2017, **655**, 117–123.
64 H. Fan and R. Yang, *J. Therm. Anal. Calorim.*, 2014, **116**, 349–357.
65 Z. Zhang, G. Liang and T. Lu, *J. Appl. Polym. Sci.*, 2007, **103**, 2608–2614.
66 K. Ghani, M. H. Keshavarz, M. Jafari and F. Khademian, *J. Therm. Anal. Calorim.*, 2018, **132**, 761–770.
67 O. E. Zhuravlev, V. M. Nikol'skii and L. I. Voronchikhina, *Russ. J. Appl. Chem.*, 2013, **86**, 824–830.
68 J. A. Gamelas, F. A. S. Couto, M. C. N. Trova˜o, A. M. V. Cavaleiro, J. A. S. Cavaleiro and J. D. P. De Jesus, *Thermochim. Acta*, 1999, **326**, 165–173.
69 P. S. Zhao, Z. R. Zhao, F. F. Jian and L. D. Lu, *J. Korean Chem. Soc.*, 2003, **47**, 553–558.
70 M. Falk, *Spectrochim. Acta, Part A*, 1984, **40**, 43–48.
71 A. Chaudhari, *Int. J. Quantum Chem.*, 2010, **110**, 1092–1099.
72 V. Crupi, D. Majolino and V. Venuti, *J. Phys.: Condens. Matter*, 2004, **16**, S5297–S5316.